

Accepted 11/22/11 for Publication in *Corrosion Science*

Kelvin Probe Electrode for Contactless Potential Measurement on Concrete – Properties and Corrosion Profiling Application

Alberto A. Sagüés^{a,b} and Michael T. Walsh^a
^a Department of Civil and Environmental Engineering

University of South Florida

Tampa, FL 33620, USA

^b Corresponding Author; sagues@usf.edu; Phone (813) 974 5819; Fax (813) 974-2957; Postal Address: Department of Civil and Environmental Engineering, ENB118, University of South Florida, 4202 E. Fowler Ave., Tampa, FL 33620, USA

Abstract

The practical feasibility of Kelvin Probe measurement of potential of the concrete surface was demonstrated. The measurements require no contact between the reference element and the concrete. Potential readings when placing the probe on dry concrete were nearly instantaneous and highly stable, in contrast with considerable potential drift with a conventional wet-tip electrode. The probe output was only modestly sensitive to the reference element working distance. The shape and range of potential profiles measured with the probe on

concrete with locally corroding reinforcement were consistent with those using a conventional wet-tip reference electrode, both identifying the anode location.

Keywords: A. steel reinforced concrete; B. polarization; C. potential parameters.

1 Introduction

The electric potential distribution on the external surface of concrete can be indicative of various ongoing processes of interest. For example, surface potential mapping is often conducted to identify the location of corroding reinforcing steel. For that application potential measurements are normally conducted by connecting the positive terminal of a high impedance dc voltmeter to the reinforcing steel assembly, and the other terminal to the metallic terminal of a reference electrode, usually a copper-copper sulfate electrode (CSE). The electrolyte end of the reference electrode is then placed in successive contact with an array of points on the external concrete surface, and the potential for each point is recorded. The resulting potential map provides a diagnostic of the presence and position of regions of the reinforcement assembly with high likelihood of ongoing active corrosion. The method [1-3] relies on the sizable potential transition (e.g. from ~ -150 mV to ~ -400 mV CSE) that formerly passive steel often experiences upon the onset of active corrosion [4,5]. Thus, regions

displaying negative potentials in the order of several hundred mV vs. CSE may be considered suspect of ongoing active corrosion. If active corrosion affects only a portion of the steel, the potential is not uniformly highly negative on the concrete surface because of the finite resistivity of concrete that joins the active and the passive portions of the assembly. The steel in the latter is only partially polarized and potential measurements against nearby concrete remain only mildly negative, so the external potential map can reveal the location of the corroding zones as well. Because of measurement artifacts described later, the measured potentials may be more or less globally offset from those in an ideal case. Thus, identification of corroding regions often relies more on consideration of potential gradients rather than of the absolute potential values.

Concrete surface potential measurements are also routinely conducted to monitor cathodic protection systems, assess the effectiveness of corrosion repair patches, and as part of electrochemical corrosion rate measurements. The latter are estimated by polarization measurements, where the amount of impressed current needed to achieve a small potential change is determined. The current is impressed by means of an additional external electrode attached to the concrete surface [4] or by means of rebar not in metallic contact with that being tested [6]. Within certain limitations [4,7,8], the ratio of potential change to impressed current density yields the polarization resistance R_p which is related to the corrosion current density i_{corr} through the Stern-Geary parameter B by the

equation $i_{corr} = B/Rp$. The resulting value of i_{corr} can then be related to the corrosion rate of the steel by the usual Faradaic conversion [9].

Surface potential measurements are sensitive to the condition of both the bulk of the concrete and its surface. For example, the presence of a carbonated concrete skin, even if it is very thin, can result in an appreciable potential difference (e.g. as much as 200 mV) between the outer surface and the bulk of the concrete [10, 13]. That difference reflects the widely different pH of pore water in the outer and inner regions. A diffusion potential (a general term that includes junction and membrane potentials as well as those resulting from other electrokinetic effects [13]) develops to preserve charge neutrality upon coupled diffusion, across the region joining both zones, of anions (OH^-) and cations (K^+ , Na^+) that have significantly different diffusivities. Weathering, sulfate attack and other environmental interactions may cause similar electrochemical potential gradients that may affect the surface potential pattern. A very dry concrete surface may prevent accurate potential determination as the effective contact resistance begins to approach the value of the voltmeter input resistance. The sensitivity of the potential measurements to these phenomena creates both an opportunity for their characterization and a concern as a source of artifacts in corrosion condition determination.

The extent to which potential measurement artifacts are present is obscured by the disruptive nature of the electrochemical reference electrode,

which requires a shared electrolyte link between the metallic terminal and the concrete pore water. When the electrolyte tip of the reference electrode touches the concrete surface, a liquid transport process starts that transfers some of the electrode solution into the concrete pores and vice versa. The process may range from mostly interdiffusion if the concrete pores are nearly saturated, to strong convective capillary action if the pores are nearly dry. The latter case may result in appreciable drift in the voltmeter reading as the system slowly approaches a steady state condition, likely involving the evolution of a diffusion potential pattern that includes both junction and membrane potential components [10,13]. Such drift can introduce added uncertainty on the result of the potential measurement, and significant artifacts in electrochemical corrosion rate measurements. Sometimes to partially alleviate those effects a pre-wetting procedure is used for the concrete surface before placing the reference electrode [1], but comparable uncertainty exists as to the potential variation (and its time variation) created by the intrusion of the wetting fluid to the formerly dry concrete.

Use of a Kelvin Probe (KP) electrode offers an alternative to avoid some of the artifacts noted above, by means of a contactless procedure that does not depend on a shared electrolyte, and that is inherently non-disruptive of the region sampled by the probe. To the knowledge of the authors, application of the KP to this end does not seem to have been previously conducted. In this work, macroscopic measurement of concrete surface potentials with a KP is explored.

The probe operation, performance, and application to potential mapping is demonstrated.

2 Principle of the KP operation and application to concrete

The KP determines the potential difference E between two surfaces designated as working and reference respectively. The principle of operation has been described extensively in the literature [14- 17] so only a brief review is presented here before addressing the issues specific to measurements on a concrete surface.

In the present case the working surface is a small part of the outer concrete surface, and the reference surface is the surface on one side of a macroscopically small (e.g., ~1 cm diameter) disk of a suitable metallic material, for example gold or stainless steel with a stable passive film. The disk and the concrete surfaces are a small distance h apart so as to approximate a parallel-plate capacitor configuration. The disk is connected through electronic conductors to the steel bar assembly embedded in the concrete. The steel bar surface is connected to the external surface of the concrete by an electrolytic path provided mainly by the water in the concrete pore network. Consequently the concrete and the reference surfaces are joined through an electronic and electrolytic conductive path with associated interfaces that determine the value of

E. The relationship linking electrical charge *Q* and potential difference *E* across a capacitor with capacitance *C* is

$$Q = E C \quad (\text{Eq. 1})$$

For plates with small gap the capacitance is approximated by

$$C = \varepsilon \varepsilon_0 A/h \quad (\text{Eq. 2})$$

where ε is the dielectric constant of the medium in the gap between the plates (normally air, $\varepsilon \sim 1$), ε_0 is the permittivity of vacuum and *A* is the one-sided surface area of the smallest of the plates, in this case the reference surface. Since *E* is fixed by the characteristics of the intervening conducting and interfacial chain, if *h* is changed from one static position to another the static value of *Q* needs to change accordingly as well to satisfy Eqs. (1) and (2). In the KP *h* is varied cyclically with time by attaching the reference disk to the end of an electrically insulating, longitudinally vibrating stem. Consequently *Q* changes cyclically as well resulting in an alternating current I_A circulating through the conductive path^A. If a potential source with known potential *E'* selected at will is inserted in that path (for example into a break made in the connecting wire to the rebar) the potential between the reference and concrete surface becomes $E+E'$. When $E'=-E$ the potential across the capacitor is zero and the alternating current

^AIn a dynamic condition *E* is not exactly constant due to interfacial polarization and ohmic drops caused by I_A , but its small value makes those effects correspondingly small, and they disappear anyway at the zeroing condition.

vanishes. This permits then determining the value of E by varying E' until $I_A=0$, a condition that can be reached with great sensitivity by adequate electronic amplification. The zeroing process can be made manually or performed automatically and promptly with ordinary control circuitry, yielding an immediate record of the value of E .

With interfaces having well-defined boundaries and locally uniform electric charge profiles, the potential E measured by the KP is the difference between the Volta (outer [15,18]) potential ψ_R of the reference surface and the Volta potential ψ_W of the working surface being examined

$$E = \psi_R - \psi_W \quad \text{Eq.(3)}$$

The metallic reference disk generally approximates those conditions and may be considered to have a well-defined spatially averaged ψ_R value. The concrete facing it is quite heterogeneous, as is the distribution in its pore network of the electrolyte responsible for much of the electric charge configuration in the material. Hence ψ_W should be considered only as an effective value, that of an ideal conductor that would yield the same experimental results as those obtained with the concrete. Thus ψ_W may be viewed as representing an approximate

average of the potential of the surface of the concrete beneath the footprint of the of the reference surface disk. Lateral heterogeneity up to the mm scale (pore space-paste-fine aggregate domain) is expected to be reasonably averaged beneath the disk, but some sensitivity to the distribution of the coarse-aggregate, which is typically >1cm in size, can be anticipated.

The value of E measured by the KP is determined by the present system as schematically described in Figure 1. The reader is referred to the treatment by Leng [17] for a thorough discussion on accounting for potentials at multiple interfaces in a KP measurement. For simplicity, only two different metals are assumed to be involved, one for the reference surface (R) and one for the steel bar (S). The respective inner (Galvani [18]) potentials are designated Φ_R and Φ_S with a corresponding interfacial potential difference $X_{SR} = \Phi_R - \Phi_S$. The arrows in the figure indicate that the stated difference of potential is added to the potential at the tail to obtain that at the head. Designations for the medium-air interfacial potential differences are respectively $X_{AR} = \Phi_R - \psi_R$ and $X_{AW} = \Phi_W - \psi_W$, and for the metal-electrolyte interfacial potential $X'_{WS} = \Phi_S - \Phi'_W$. Both Φ_W and Φ'_W are effective magnitudes representing a similar idealization as that noted above for ψ_W . The values of Φ_W and Φ'_W are in general not the same because of the ohmic potential drop created by the corrosion macrocell currents in the concrete, and of electrolyte composition gradients within the concrete that cause macroscopic junction potentials and electrokinetic effects [12,13]. These factors

will be further considered later on. The resulting difference is designated as $\Delta\Phi_W = \Phi'_W - \Phi_W$. Ohmic drops and similar effects within the metals themselves are treated as negligible in the present analysis. Applying the above definitions to Eq. (3) yields

$$E = X'_{WS} + X_{SR} - X_{AR} + X_{AW} + \Delta\Phi_W \quad \text{Eq (4)}$$

A similar representation and nomenclature is presented in Figure 2 for a conventional measurement of steel potential vs. a regular reference electrode using a high impedance voltmeter [18]. For simplicity, it is assumed that a Cu-CuSO₄ electrode (CSE) is being used and that all the connections involve Cu wiring, including the terminations of the voltmeter. In such case the Galvani and Volta potential differences between the voltmeter leads are the same, and the measured potential E_{CSE} is given by

$$E_{CSE} = \Phi_{Cu1} - \Phi_{Cu2} = X'_{WS} + X_{SCu} - X_{BCu} + X_{BW} + \Delta\Phi^*_W \quad \text{Eq (5)}$$

The salt bridge in Figure 2 is assumed to include a porous plug, as well as a wet sponge or similar accessory, between the bulk of the CuSO₄ solution in the electrode and the surface of the concrete. The potential difference X_{BW} incorporates any diffusion potentials or related phenomena associated with ionic concentration gradients across the plug and sponge. It is noted that the polarity chosen to designate X_{BCu} , a metal-to-electrolyte interfacial potential difference,

was chosen for uniformity to match that used for X'_{WS} so both variables adhere to the usual electrochemical convention.

Given its contactless character, placement of the KP on the system should create no significant change of X'_{WS} and $\Delta\Phi_W$ from their native values. Placement of the CSE and sponge should likewise be expected to have little effect on the value of X_{WS} , at least when the concrete cover is not very thin and only moderate surface wetting is involved so the macrocell pattern is not substantially affected. However, the CSE placement is more disruptive of conditions near the external concrete surface. The concrete pore network in the contact region and to some distance beneath it is expected to be affected by intrusion of water and ions coming from the reference electrode and accessories, and from any pre-wetting applied to the surface of the concrete. As indicated earlier the potential distribution in that region is altered to some extent relative to the initially dry condition, so Φ^*_W and $\Delta\Phi^*_W$ are used instead of the values without asterisk in the undisturbed case in Figure 1.

The relationship between E and E_{CSE} is discussed next. From Eqs. (4) and (5) and treating X'_{WS} as being invariant as indicated earlier, the potential measured by the KP can be related to that measured in the usual manner with a CSE reference electrode by

$$E = E_{CSE} + [(X_{SR} - X_{SCu}) + (X_{AW} - X_{AR}) + X_{BCu} + \Delta\Phi_W] + [-X_{BW} - \Delta\Phi^*_W] \quad \text{Eq.(6)}$$

The terms grouped within the first set of square brackets are functions of the properties of metal-metal, metal-air and metal-solution interfaces, and of the condition of the concrete in the undisturbed condition. Those quantities may then be considered on first approximation as being constants of the system and together contribute as a simple constant addition term to the conversion between E and E_{CSE} , at least for the particular place on the concrete surface being examined. In contrast, the terms within the second set of square brackets depend on the time evolution of the system as moisture and ionic species penetrate in the region contacted by the wet-tip electrode and sponge, and affected by pre-wetting. Thus those terms are time-dependent and their effect on the total amount is to preclude relating E and E_{CSE} through a simple time-invariant addition term. The variation should become very slow after a steady state moisture and ionic species distribution is reached, but those processes may take a long time [10]. In practical terms, for comparing KP and conventional wet-tip electrode measurements it is best to examine the system after a prearranged time after surface wetting started, when the time dependent terms have evolved to a roughly reproducible extent. That approach was adopted in the experiments presented here.

The above analysis can be extended to compare the case of KP measurements on a pre-wetted concrete surface with those performed conventionally on an equally pre-wetted surface. In that case both X_{AW} and $\Delta\Phi_W$

become time-dependent as well, although $\Delta\Phi_W$ may be closer to $\Delta\Phi_W^*$ so the contribution of that pair could cancel to some extent. On the other hand pre-wetting can also affect X_{AR} due to adsorption of water on the reference disk due to evaporation from the freshly wet concrete surface^B. Thus, timing of the KP measurement with respect to the moment of pre-wetting needs to be noted as well for comparison between KP and conventional measurements when both involve a pre-wetted surface.

These considerations can be readily extended to any other reference electrode besides the CSE, with appropriate substitution for X_{SCu} and X_{BCu} and for introduction of any pertinent additional metal-metal contact. The other terms and their significance remain the same as before.

Experiments were conducted here to determine the feasibility, sensitivity to system variables and stability of KP measurements on concrete surfaces, and the extent to which the results could be correlated to conventional measurements in the context of the above discussion.

^B In lieu of a more sophisticated treatment that would need to address the creation of other interfaces due to the formation of a film or deposit, the combined effects are bundled for simplicity as an equivalent change in the effective value of X_{AR} . The same approach applies here to any electrode that has a passive film or any other compositional differences near the surface.

3 Methodology

A KP was constructed with a 13 mm diameter austenitic stainless steel (Type AISI 302) reference disk vibrating at 147 Hz with an approximately sinusoidal, waveform of amplitude $h_A = 0.5 \pm \sim 0.1$ mm (i.e., $1 \pm \sim 0.2$ mm peak-to-peak), implemented using a voice coil electromagnetic driver. At rest the reference to working surface distance was $h = 1$ mm, so the closest nominal reference-to-working surface distance was $h_C = h - h_A = \sim 0.5$ mm. The disk surface was ground to an 800-grit finish and periodically cleaned by gently brushing with a cotton-tipped applicator wetted with ethyl alcohol. The disk was placed at the end of a short stem made of wood, to better dissipate static charging. As shown in the sketch and photograph in Figure 3, a perforated metal casing placed around the vibrating assembly and preamplifier provided shielding, leaving a 4 mm gap between the casing skirt and the concrete surface. Three insulated stop screws around the skirt perimeter forming a triangle with the disk inside ensured stable positioning against flat surfaces, and permitted fine h adjustment when needed. The adjustment was to ± 0.1 mm of the desired value, by gaging against a flat machined surface. The experiments were only performed against nominally flat and smooth concrete surfaces which typically introduced < 0.1 mm additional uncertainty in the value of h . However, probe design could easily be optimized for more compact size and automatic working distance adjustment using well established technology. The sensing circuit detected the off-zero current with a circuit that approached a zero-resistance-ammeter configuration

[14]. Zeroing was made automatically with a feedback circuit, and the value of E was acquired digitally. The probe output was electronically filtered with a low pass filter with time constant $\tau \sim 1$ s.

Concrete prisms 5 cm thick, 15 cm wide and 70 cm long were made in duplicate using the mixture proportions listed in Table 1.

Table 1 – Mixture Proportions

Constituent	Description	Amount
Cement	Type I/II	339 kg/m ³
Coarse Aggregate	Limestone ~ 2 cm max.	1,017 kg/m ³
Fine Aggregate	ASTM C778 Graded Sand	678 kg/m ³
Water (W/C=0.5)	Tap Water	169 kg/m ³

The central 50 mm of the prism contained 8.4 kg/m³ Cl⁻ ion (2.5 wt% of the cement content, exceeding typical corrosion initiation threshold levels [19]) admixed by adding the corresponding proportion of NaCl (13.9 kg/m³). Removable dams separated the Cl⁻ - admixed region from the rest while casting the concrete; the dams were removed just before final consolidation resulting in a continuous joint. Wooden molds with a thin mold release cover were used. The

slabs were cast so that five surfaces were form-cast and the remaining one (a broad face) was free and hand finished.

Each specimen had a longitudinally centered #4 (13 mm diameter) plain steel ASTM A-615 reinforcing steel bar with dark mill scale, with the last 13 mm inside concrete on each end as well as any emerging steel covered with epoxy to avoid exit line corrosion. Steel placement is shown in Figure 4.

All KP and conventional wet-tip electrode tests were performed on the broadest form-cast surface of the specimens. The form-cast surfaces were macroscopically flat, but finely rough as is typical of a wood form finish.

The specimens were covered to prevent evaporation and demolded ~ 4 days after casting. Curing inside plastic bags with excess water continued until 4 weeks after casting, after which the specimens were left exposed to laboratory air, ~60% relative humidity (RH) and ~ 24C. Initial conventional surface potential surveys confirmed the presence of an actively corroding central region on the rebar, coinciding with the chloride contaminated concrete. However, potential differentiation between the central anodic region and the rest of the surface was only modest (e.g < 150 mV) and tended to lessen with increasing drying of the specimens. To increase differentiation, after ~12 weeks of exposure to laboratory air the specimens were re-moisturized in closed wet bags for ~2 weeks. The specimens were then modified on the hand-finished surface (on the opposite side where the potential measurements were made) by drilling in the chloride-contaminated zone with a masonry drill three equispaced 1-cm diameter holes,

just reaching the rebar surface. Approximately 1 cm³ of NaCl-saturated water was placed in each hole and allowed to partially absorb in the surrounding concrete. The holes were filled with paper soaked with the same solution and covered with duct tape. Measurements conducted during the following 1-2 weeks on the opposite form-cast surface revealed >200 mV potential differentiation in the potential profiles of the two duplicate specimens. The potential measurements reported here correspond to that period.

Potential profiles were obtained with the KP on the dry and pre-wetted concrete surface conditions, and with a conventional reference electrode on the pre-wetted concrete surface condition as well as on dry concrete for selected tests. The conventional electrode was a saturated calomel electrode (SCE). This electrode was chosen instead of the CSE commonly used for concrete tests, to rule out any possible artifacts from the CuSO₄ stains often left by the later. The SCE uses a fine glass frit electrolyte channel that allows only vestigial KCl contamination, while having low enough impedance to be unaffected by the FET-input front end of the data logger system used with that electrode. The tip of the SCE was surrounded by a 3mm-thick sponge sheet wetted with tap water of ~2 k ohm-cm resistivity. For the pre-wetted condition measurements the surface of the concrete was dabbed on the test spots with a tap-water-soaked sponge. Any free surface water was blotted off. As indicated in the previous section, the overall provisions in comparing measurements from KP and conventional measurements still apply if the SCE is used instead of the CSE.

Potential profile measurements were performed on the broad form-cast surface, on top of the rebar, at the center of the face and at 2.5 cm intervals on either side for the SCE and 1.25 cm intervals for the KP. The probe or electrode output was recorded with a data logger ~5 seconds after placement in the test spot.

For profile measurements on the dry surface condition the specimen had been allowed to dry in lab air overnight from any previous test involving wetting. For pre-wetted condition profile measurements the SCE or KP was placed and the potential read on each spot typically within ~20 s after the spot was prewetted. Repeat potential profiles were conducted ~10 minutes after the first.

4 Results and Discussion

4.1 Stability of Potential Readings

When placed on an undisturbed concrete surface in steady atmospheric contact, the KP provided nearly instantaneous and far more stable readings than those possible with a conventional wet-tip reference electrode. Figure 5 shows typical time records of the output of the KP following placement on the surface of a reinforced concrete specimen that had been left in laboratory air for several

days/weeks after curing. The tests were conducted at least one day after any previous temporary wetting of the surface for SCE measurements. The records correspond to transfer of the probe onto the concrete surface from rest on another point on the concrete surface that had a different potential. Primary stabilization to the new potential took ~1 second, reflecting the time constant of the electronic filtering circuit. The charts show the potential drift as change of output relative to the value obtained at a moment 1 second after probe placement in the new position. That moment was designated as time=0. The output for time>0 remained constant typically within ± 1 mV for an evaluation period of 3 minutes as long as the probe sensing disk assembly and underlying concrete surface remained undisturbed. Warm or moist air briefly blown on the sensing area caused potential excursions of up to several mV that vanished a few seconds after the disturbance ended.

Figure 5 also shows for comparison the potential evolution observed when placing afterwards on the same point the SCE with its wet sponge tip, but without prewetting the surface. As it is commonly observed in such cases [1,10], there was considerable drift of the output, reflecting electrolytic rearrangement in the pore network of the concrete near the surface as it is invaded by the water from the sponge, with consequent slow establishment of a new diffusion potential regime. In the context of Eq. (5), those changes reflect variations in $\Delta\Phi_w^*$ and X_{BW} . The causes and direction of those changes are addressed in the discussion on potential profiles later on. The extent of drift (e.g., up to >40 mV in 3 minutes)

greatly exceeded that encountered with the KP and in most instances the output had not visually stabilized during the recording interval. Further considerations on output stability are given in subsequent sections.

4.2 Effective Working Surface Position

For media with sufficient presence of mobile charge carriers the position of the working surface from the standpoint of the operation of a macroscopic KP is effectively the same as the geometric outer surface of the material [16]. For a porous material like concrete, electric charge transport is dominated by the pore solution which normally is highly conductive and partially fills the pore network. The solid aggregate – cement paste matrix has properties that approach those of a porous dielectric with vestigial conductance. For moist concrete, appreciable amounts of pore water are expected to exist right up to the concrete outer surface so it is clearly the working surface. For concrete long exposed to air of moderate relative humidity the electrolyte presence in the pore network may be very small due to evaporation, and the conductivity of the remaining electrolyte may be also much diminished due to reaction with atmospheric CO₂. Depending on the concrete age and external humidity those effects reach depths ranging from only a few μm to as much as many cm [4]. It was desired to determine to which extent the KP working surface coincided with the geometric outer surface for concrete in various conditions.

To examine that issue, measurements were conducted with the KP zeroing circuit intentionally deviated, by 1 V, out of the balance condition. In that condition the alternating current generated by the probe has its main spectral component with frequency equal to the vibrating frequency, and amplitude approximately inversely proportional to h_C [20]. The KP circuit reports that current after amplification as an a.c. potential, of which the r.m.s value, V_{OB} , was measured and recorded. When the effective working surface coincides with the outer material surface, a plot of V_{OB}^{-1} as function of h should yield a curve that on extrapolation intersects the h axis at $h = h_A$ since at that condition the reference surface would virtually contact the working surface with ideally unlimited output amplitude. If the effective working surface were deeper than the external surface, the extrapolated intersection of the curve for $V_{OB}^{-1}(h)$ with the horizontal axis would be at a value lower than h_A , with a consequent expected shift of the curve to the left compared with the previous case.

As a baseline, the value of V_{OB} was measured when the KP reference was placed on a flat-machined smooth steel surface at the normal $h = 1\text{mm}$ working distance, and also after increasing h to 1.25, 1.5, 1.75 and 2mm. The same procedure was conducted at various points on the surface of the concrete prisms when they had had been left in laboratory air for several days/weeks after curing. Similar tests were conducted with three other available reinforced concrete specimens that had been allowed to dry in laboratory air for over a decade after a

previous investigation. The composition of the concrete in those specimens corresponds to mixes A, E and F as detailed elsewhere [21].

Figure 6 shows the resulting $V_{OB}^{-1}(h)$ graphs. The results for steel could be closely fit to a second-degree polynomial relationship with modest quadratic component. The h-axis intercept of the fit function (average of two tests) was ~ 0.56 mm, approaching the value of $h_A = 0.5$ mm expected for a metallic surface closely, considering the 0.1 mm uncertainty affecting both h and h_A . The curves for concrete, regardless of composition or age, all deviated very little from the shape and position of the curve obtained for steel. Because of the close superposition, only variation bands are shown, indicating the range of V_{OB}^{-1} values obtained for the concrete specimens. The greatest corresponding leftward horizontal deviation from the steel curve was only ~ 0.1 mm, which is well within the overall variability in h especially since in concrete specimens some surface deviation from a fully flat surface is common. The h-axis intercept of the fit for the concrete specimens was virtually the same as that for the steel surface. It was thus concluded that the concrete geometric outer surface coincided with the KP working surface, at least within the operating positioning precision. That result applied even for concrete that had aged extensively under the type of moderately dry atmospheric conditions that lead to high surface resistivity values (e.g. $> 1 \text{ M}\Omega\text{-cm}$).

4.3 Sensitivity to Working Distance

Spurious surface and spatial electric charges exist in the supporting structure and other conductors near the vibrating disk inside the shielding enclosure. Those charges modify the electric field created by the working surface, so that the nulling potential differs from that which would have been obtained in the absence of the spurious sources. The effect is relatively stronger the further away the disc is from the working surface, so the result of the KP measurement becomes sensitive to the average probe-to-working surface distance [20]. The extent to which this artifact existed in the present system was determined by varying the distance between the probe supports and the concrete surface by means of spacers and measuring the resulting change in output.

The effect was found to be small, in the form of a shift in measured potential in the positive direction typically ranging from nil to <40 mV when increasing h from 1 mm to 2 mm, a change much larger than the usual variability of h . Within that 1mm range the precise magnitude of the shift varied depending on recent history of maintenance of the disk supporting assembly and cleaning of the internal surface of the shielding enclosure. For any given such condition the shift was approximately linearly dependent on the increase in working distance, and of the same order when measuring either a flat-machined smooth steel surface or concrete. Refinement in future probe design is expected to readily minimize residual sensitivity to working distance.

4.4 Potential Profile Measurements

This section addresses potential measurements conducted at various points of the concrete surface over a single piece of reinforcement with various polarization conditions along its length. Before addressing those results it is noted that other tests were conducted with the KP placed at a fixed position on the dry surface of the specimens that had multiple, non-interconnected metallic electrodes (the same specimens from a previous investigation noted earlier). In those tests the KP yielded, as expected, potential values for the various electrodes that differed from each other by the same amount as that determined by direct measurement with a high impedance voltmeter. The agreement was within the $\pm 1\text{mV}$ resolution and overall percent accuracy of the digital displays of the voltmeter and the KP, as long as the switching of the KP connection from one electrode to the other was performed promptly so minor drift effects such as those shown in Figure 5 did not introduce additional error.

Figure 7 shows potential profiles obtained with the KP and with the SCE for each of the duplicate longitudinal rebar specimens. The results correspond to the condition described earlier, shortly after modification on the backside of the specimens to obtain a strongly evidenced central corroding region. In each specimen the first set of measurements was taken in the dry surface conditions with the KP, proceeding from one end of the slab to the other and then repeated immediately. The surface of the slab was then topically moistened at the

intended test spots and a second set of duplicate measurements was taken using the SCE with the wet sponge tip. Afterwards the surface topical moistening was refreshed and a final set of duplicate measurements was taken on the moist spots with the KP. The duplicate results for the three sets of measurements are labeled KP-Dry, SCE Wet and KP-Wet respectively.

The results from both slabs were comparable within the variability levels commonly encountered with assessing corrosion phenomena in concrete. The following addresses the short term repeatability in immediately consecutive profile measurements within a given slab, and the overall features of the potential profiles.

Regarding short term repeatability, the KP-Dry data showed closely overlapping consecutive profiles along the entire length of the specimen, consistent with the nearly constant output noted in Figure 5 for the KP placed on a stabilized dry concrete surface. The SCE Wet data showed greater variability in consecutive results than those for KP-Dry data, reflecting spot-to-spot variations in time-dependent water absorption and evaporation following the pre-wetting. The changes, which can be interpreted as noted earlier in the context of Eq. (5), were in the same order as those shown in the time charts in Figure 5 for the SCE data after the first minute or so of placing the wet sponge on a previously dry concrete surface. When the KP was placed on the pre-wetted locations the consecutive measurements on the same spot showed variability

greater than that for the KP in the dry condition, and comparable to that in the SCE Wet data. As in the SCE measurements, that variability is interpreted as being associated with moisture evolution with time at the pre-wetted spots on the concrete surface, affecting X_{AW} and $\Delta\Phi_W$. Also as noted earlier, minute changes in the amount of water adsorbed on the reference disk surface, given its proximity to the freshly evaporating concrete surface, may have contributed to the variability as well through changes in X_{AR} .

Regarding overall features, the SCE profiles showed the distinct negative dip pattern, in the present case ~200 mV deep, expected from a concrete slab with a centrally corroding segment on a longitudinal reinforcing bar [22,23]. Figure 7 shows that the KP profile shape and range, for both the dry and wet conditions, generally reproduced the SCE pattern. That is manifested in the graphs in Figure 8 that show linear correspondence with slopes ranging from 0.87 to 1.12 and correlation coefficients ranging from 0.87 to 0.96. The corresponding offsets from an ideal 1:1 coincidence with the CSE readings were about +100 to +200 mV for the KP-Dry condition, and about half as much for the KP-Wet condition. Comparison of the profiles is conceptually more straightforward for the Wet cases, where both probes interacted with a concrete surface in the same nominal condition and measurement timing was similar. Assuming on first approximation a correlation slope of unity, the potential offset for the wet cases may be viewed as a temporary calibration of the KP readings with respect to potential measurements in the SCE scale, corresponding ideally

to the addition of the terms in square brackets in the equivalent of Eq.(6) for an SCE.

The calibration should be viewed as temporary because even if the timing of the measurements with respect to the moment of wetting were strictly controlled, day to day variations in environmental variables as well as long term evolution of the concrete surface are expected to appreciably affect the key parameters in Eq.(6). In particular, the value of X_{AR} (as treated in the simplified treatment used here) is highly sensitive to the makeup of a region only a few atomic distances thick on the disk surface. Even if the disk had been recently cleaned, monolayer-levels of moisture or organic vapor precipitation on the surface can readily build up with time of exposure to normal environmental conditions, leading to potential changes that can be large (e.g. > 100 mV [14]). Variations of that order were noted during testing conducted at different times, especially if servicing of the probe disk was involved. Consequently, if absolute as well as relative potential profile information were sought with the KP, a fresh calibration step should be conducted concurrent with the measurements. It is also reminded that the potential offset depends on the nature of the disk alloy used, so the relative position of the data graphs in Figure 8 would have been different if, for example, a gold-plated would have been used instead of the stainless steel disk.

The KP-Dry surface profiles were, as exemplified in Figures 7 and 8, usually positively offset with respect to those obtained in the Wet condition. This shift is in the same direction as that documented for the SCE in Figure 5 by

comparing the potential obtained at very short times, when the concrete surface was only beginning to depart from its initial dry condition, to the more negative values prevalent after substantial water absorption from the sponge took place. Such change may be interpreted as due to the slow dissipation of a diffusion potential (manifested in the combined values of X_{AW} and $\Delta\Phi_W$ or X_{BW} and $\Delta\Phi_W^*$ in Eqs. (4) or (5) respectively) due in part to a gradient in OH^- concentration in the water partially filling the pores [10,13]. The OH^- concentration of the pore water has high values inside the concrete, due to high alkaline content [24], and smaller values near the surface because of carbonation by interaction with atmospheric CO_2 . In this interpretation, the higher diffusivity of the OH^- ions compared with that of the balancing cations [13] promotes a diffusion potential difference where the outer surface is more negative than the inside; because of the polarity of the KP and SCE measurements the result is a more positive steel potential reading than if the diffusion potential were not present. Other electrolytes, such as those associated with chloride salts, would have additional individual effects. As water refills the partially empty pore network near the surface, the resulting enhanced transport between outer and inner regions lessens solute concentration gradients hence reducing the magnitude of the junction potential difference and resulting in a shift in the negative direction of the measured potential.

The KP-Dry surface profiles showed also more spatial variability than those for the Wet condition. Because of the high reproducibility noted above, the

spatial variability represented in general true local potential differences on dry regions 1.25 cm apart. The source of the short distance variability is yet to be identified in follow up work. In that context, it is noted that the KP-Wet profiles tended to show less short-distance spatial variability than for the dry condition. It may then be proposed that the local variations in the dry case are associated with variations in diffusion potential from local changes in the degree of carbonation, or differences in the evaporative concentration at the extreme outer surface of other species with similar outcome. Some of the differences may be associated with how close to the surface the coarse aggregate may be locally. Those effects would diminish upon pre-wetting as discussed earlier, resulting in a smoother potential profile than that in the dry condition.

The above discussion generally assumed that the moisture condition of the steel-concrete interface was the same while switching between the dry and wet conditions of the outer concrete surface over short periods of time. The changes were considered to be negligible because the concrete slabs were relatively young and had also experienced periodic moisture conditioning. In those conditions and for the 0.5 w/c concrete used, convective transport is expected to be limited to a depth from the surface appreciably less than the concrete cover thickness over the rebar [25]. Transport by diffusion through the pore network of the concrete is very slow and it would not be expected either to lead to any noticeable effects on the time scale considered [4]. Hence the results from both the dry and wet surface experiments were interpreted to differ primarily

because of changes in the zones closer to the outer concrete surface. The moisture content at the rebar surface could however change substantially on external moisture cycling if cover were shallower or the cycles longer. In such cases the potential difference between the two conditions observed with the KP could include also a component due to variations in the potential across the metal-pore water interface, not unlike those encountered between immersed and emersed conditions in passive metals [26].

The profile measurements presented here were exploratory in nature, and addressed for simplicity cases with strongly defined corrosion macrocell patterns that dominated the potential distribution on the concrete. The partial contribution resulting from the chloride content gradient, which can also indirectly affect the local rate of carbonation, is being investigated in follow up work. Further work should also aim toward development of a rational calibration procedure to relate the potential determined by the KP to that of the metal-concrete interface, perhaps by adequate choice of an external concrete surface condition and a methodology comparable to that of Leng [17].

4.5 Prospective applications and open issues.

This work demonstrated the practical feasibility of KP measurement of potential on the concrete surface, with very low drift on dry concrete surfaces, and sufficient sensitivity for detailed potential mapping. An especially attractive

feature of the KP is its ability to perform essentially instantaneous and non-intrusive measurements, requiring neither direct contact with the surface nor prior surface preparation in the form of wetting plus stabilization. The output sensitivity to disk-to-surface distance is modest, which is desirable for practical use on regularly finished concrete surfaces. Some prospective applications for continuing investigation are noted next.

The KP merits consideration as an alternative to wet-tip contacting reference electrodes for conducting potential survey of bridge decks or similar structures without need for laborious maintenance of wet contacts [1, 2]. Given its speed, stability and absence of contact with the concrete surface the KP or an array thereof may be particularly suitable to adapt for automatic operation trailed from a slow moving vehicle for minimum traffic disruption. Future work to assess the feasibility of this application should determine how tolerable is the measurement scatter introduced by the probe sensitivity to the surface condition of itself and of the concrete, especially in the presence of contaminant spills or other commonly occurring alterations of the structural surface. Some of that scatter, as well as the sensitivity to surface roughness, may be reduced by using a larger reference disk and a higher disk-to-surface distance. Those modifications provide for spatial averaging of the output with consequent filtering of short-distance variations, and can be implemented by hardware scaling with readily available technology. In addition, control of the condition of the disk

surface will need attention, including possible use of solid alloys or surface plating less prone to contamination.

The KP probe also holds promise as a highly stable reference electrode for measurements of polarization resistance or of low frequency electrochemical impedance of reinforcement, especially when the concrete surface is dry and it is desired not to disturb it. In those cases wet-tip electrode potential drift, as well as the effect of any moisture applied to the concrete near the reinforcement for surface preparation, could lead to appreciable measurement artifacts. The use of the KP together with a non-wetting counter electrode (such as a conductive elastomer [27]) would obviate those concerns. Polarization tests of this type involve measuring only relative potential changes at a single point on the surface, so sensitivity to spatial variations in concrete surface condition is not an issue such as it was for potential mapping. Application of the KP to this type of measurement has been demonstrated for other systems [28]. Experiments to demonstrate feasibility for the present case are in progress.

In its present form the probe would require, for either of the above applications, a ground contact to one point in the normally electrically continuous reinforcing steel assembly of the structure to be assessed. For traveling probes that connection should be implemented beforehand, so the entire structure could be sampled using a temporary flexible extension cable. In potential mapping the identification of corroding spots may be sufficiently established, if the surface

potential gradients are large enough, solely by means of differential potential measurements which ideally do not need a ground contact. That approach can be implemented with wet-tip reference electrodes if they and the underlying concrete have sufficiently low impedance to keep electrical noise at acceptable levels. The feasibility of a similar approach using a differential KP configuration needs yet to be established by conceptual development and demonstration.

For clarity, it is noted that the use of the KP as introduced here focuses on avoiding the need for contact with the concrete surface at the potential test point. Technology has been introduced recently for corrosion assessment by polarization measurements with current injection and extraction points with contacts on the concrete surface, but none to the rebar assembly [29]. That technology addresses a different issue not to be confused with that of the present paper, although it may be possible in the future to favorably combine aspects of each.

While a source of scatter in the case of potential mapping applications, the high sensitivity of the KP to the condition of the concrete surface offers a powerful alternative to investigate phenomena for which a wet-tip electrode would be too disruptive. Among other applications, the KP with appropriate customization may be able for example to (i) measure the evolution of the early stages of concrete carbonation in real time by monitoring the associated diffusion potential development, a sensitivity that applies also to the following; (ii) detect

moisture content gradients that would have been otherwise overwhelmed by contact with a wet electrode tip; (iii) detect diffusional penetration and partition of moisture and chemical species such as chloride ions between aggregate and hydrated cement paste in concrete cross sections; (iv) assess the transport and distribution of migrating corrosion inhibitors in concrete; (v) characterize the penetration and aging of concrete surface treatments such as silane/siloxane compounds; (vi) characterize the extent of evaporative concentration of species such as chloride ions on the external concrete surface; (vii) assessment of sulfate attack; (viii) assessment of concrete surface contamination and the effectiveness of cleaning and remediation methods.

6 Conclusions

The practical operation of a macroscopic Kelvin Probe (KP) for contactless measurement of concrete surface potentials was demonstrated.

Potential readings when placing the KP on dry concrete surfaces were nearly instantaneous and highly stable, in contrast with the considerable potential drift that took place when first placing a wet-tip electrode on the same surfaces.

The potential sampled was found to be that of a plane closely approaching the outer concrete surface even for concrete specimens that had been exposed

to dry and naturally carbonating lab air for many years, for which high surface resistivity is expected.

The KP output was only modestly sensitive to changes in the reference disk to concrete surface working distance.

The shape and range of potential profiles measured with the KP were consistent with the location of the local anode in a reinforced concrete beam with a well-differentiated centrally corroding rebar segment. The KP profiles were offset from, but comparable in shape and range, to those obtained independently with a conventional wet-tip reference electrode. The offset depended on the condition of both the KP disk and the concrete surface, so appropriate calibration is needed if absolute potential determination with the KP is desired.

Comparable KP profile features were obtained when sampling the concrete in either the dry or a pre-wetted surface condition, but with greater point-to-point variability in the former. The variability reflects the sensitivity of the KP output to the local condition of the concrete surface. That sensitivity may be caused by the development of ionic concentration gradients with depth from the concrete surface, with associated diffusion potential differences.

The results encourage exploration of the use of the KP for fast automated field corrosion potential surveys, precise polarization and electrochemical

impedance determination when the concrete surface is dry, and physicochemical determinations in concrete for conditions where the use of a conventional wet-tip reference electrode would be disruptive.

7 Acknowledgment

This work was performed with the support and facilities of the University of South Florida. The assistance of Kingsley Lau with trial tests is greatly appreciated.

8 References

- [1] ASTM C876 - 09, Standard Test Method for Half-Cell Potentials of Uncoated Reinforcing Steel in Concrete, 2009.
- [2] B. Elsener, C. Andrade, J. Gulikers, R. Polder, and M. Raupach, Half-Cell Potential Measurements – Potential Mapping on Reinforced Concrete Structures, *Materials and Structures* 36 (2003) 461-471.
- [3] Y. Schiegg, M. Buchler and M. Brem, Potential mapping technique for the detection of corrosion in reinforced concrete structures: Investigation of parameters influencing the measurement and determination of the reliability of the method, *Materials and Corrosion* 60 (2009) 79-86.
- [4] L. Bertolini, B. Elsener, P. Pedefferri, and R. Polder, *Corrosion of Steel in Concrete*, Wiley, Weinheim, 2004.
- [5] U.M. Angst, B. Elsener, C.K. Larsen, O. Vennesland, Chloride induced reinforcement corrosion: Electrochemical monitoring of initiation stage and chloride threshold value, *Corrosion Science* 53 (2011) 1451–1464.

- [6] A.A. Sagüés, S.C. Kranc, and E. Moreno, Time Domain Response of a Corroding System with Constant Phase Angle Interfacial Component: Application to Steel in Concrete, *Corrosion Science* 37 (1995) 1097-1113.
- [7] C. Andrade and J. Gonzalez, Quantitative Measurements of Corrosion Rate of Reinforcing Steels Embedded in Concrete Using Polarization Resistance Measurements, *Werkstoffe und Korrosion* 29 (1978) 515-519.
- [8] A.A. Sagüés, M..A. Pech-Canul, and Shahid Al-Mansur, Corrosion Macrocell Behavior of Reinforcing Steel in Partially Submerged Concrete Columns, *Corrosion Science* 45 (2003) 7-32.
- [9] D.A. Jones, Principles and Prevention of Corrosion, 2nd ed., Prentice Hall, Upper Saddle River, 1995.
- [10] R. Myrdal, Phenomena that Disturb the Measurement of Potentials in Concrete, *Corrosion/96*, paper no. 339, NACE International, Houston, 1996.
- [11] R. Myrdal, Potential Gradients in Concrete Caused by Charge Separations in a Complex Electrolyte, *Corrosion/97*, paper no. 278, NACE International, Houston, 1997.
- [12] U. Angst, O. Vennesland, and R. Myrdal, Diffusion Potentials as Source of Error in Electrochemical Measurements in Concrete, *Materials and Structures* 42 (2009) 365-375.
- [13] U. Angst, B. Elsener, R. Myrdal, and O. Vennesland, Diffusion Potentials in Porous Mortar in a Moisture State below Saturation, *Electrochimica Acta* 55 (2010) 8545-8555.
- [14] U. Klein, W. Vollmann, and P.J. Abatti, Contact Potential Differences Measurement: Short History and Experimental Setup for Classroom Demonstration, *IEEE Transactions on Education* 46 (2003) 338-344.
- [15] M. Stratmann and H. Stachel, On the Atmospheric Corrosion of Metals which are Covered with Thin Electrolyte Layers – I. Verification of the Experimental Technique, *Corrosion Science* 30 (1990) 681-696.
- [16] L. Kronik and Y. Shapira, Surface photovoltage phenomena: theory, experiment, and applications, *Surface Science Reports* 37 (1999) 1-206.
- [17] A. Leng, H. Streckel, and M. Stratmann, The Delamination of Polymeric Coatings from Steel – Part 1: Calibration of the Kelvinprobe and Basic Delamination Mechanism, *Corrosion Science* 41 (1999) 547-578.

- [18] J. Bockris, A. Reddy, and M. Gamboa-Alcedo, *Modern Electrochemistry*, Vol. 2A, 2nd Ed., Kluwer Academic, New York, 2000.
- [19] Ann, K. Y., and Song, H. W., "Chloride Threshold Level for Corrosion of Steel in Concrete," *Corrosion Science* 49 (2007) 4113 -4133.
- [20] B. Ritty, F. Wachtel, R. Manquenouille, F. Ott, and J. Donnet, Conditions necessary to get meaningful measurements from the Kelvin method, *J.Phys. E: Sci. Instrum.* 15 (1982) 310-317.
- [21] E.I. Moreno, A. Sagüés, and R.G. Powers, Performance of Plain and Galvanized Reinforcing Steel During the Initiation Stage of Corrosion in Concrete with Pozzolanic Additions, *Corrosion/96*, paper no. 326, NACE International, Houston, 1996.
- [22] J. Ozbolt, G. Balabanic and M. Kuster, 3D Numerical modeling of steel corrosion in concrete structures, *Corrosion Science* 53 (2011) 4166-4177.
- [23] S.C. Kranc, A.A. Sagüés, Detailed modeling of corrosion macrocells on steel reinforcing in concrete, *Corrosion Science* 43 (2001) 1355–1372.
- [24] L. Cáseres, A.A. Sagüés, S.C. Kranc and R.E. Weyers, In-Situ Leaching Method for Determination of Chloride in Concrete Pore Water, *Cement and Concrete Research* 36 (2006) 492-503.
- [25] P. Schiessl and S. Lay, Influence of concrete composition, *Corrosion in reinforced concrete structures*, H. Boehni, Ed., CRC Press, Woodhead Publishing Ltd., Cambridge, 2005 pp. 91-134
- [26] R. Hausbrand, M. Stratmann, and R. Rohwerder, The Physical Meaning of Electrode Potentials at Metal Surfaces and Polymer/Metal Interfaces: Consequences for Delamination, *Journal of The Electrochemical Society* 155 (2008) C369-C379
- [27] M.A. Pech-Canul, A. A. Sagüés, and P. Castro, Influence of Counter Electrode Positioning on Solution Resistance in Impedance Measurements of Reinforced Concrete, *Corrosion* 54 (1998) 663-667.
- [28] G.S. Frankel, M. Stratmann, M. Rohwerder, A. Michalik, B. Maier, J. Dora and M. Wicinski, Potential control under thin aqueous layers using a Kelvin Probe, *Corrosion Science* 49 (2007) 2021–2036.
- [29] C. Andrade, I. Martínez and M. Castellote, Feasibility of determining corrosion rate by means of stray current-induced polarization, *Journal of Applied Electrochemistry* 38 (2008) 1467-1476.

Figure Captions

Figure 1 – Schematic representation of potentials and interfacial potential differences in a KP arrangement for steel in concrete.

Figure 2 – Schematic representation of potentials and interfacial potential differences in a conventional reference electrode arrangement for steel in concrete, illustrated for the CSE.

Figure 3 – Schematic and photograph of Kelvin Probe (KP) implementation.

Figure 4 – Reinforced concrete test specimen configuration and example of KP probe placement.

Figure 5 – Stability of Measured Potential for KP and SCE, shown as drift from value measured 1 second after probe placement on dry concrete. Results shown as stacked graphs for four positions indicated by distance from center of Slab A..

Figure 6 – Determination of effective working surface position. Circles: Flat-machined steel surface. Range bands: Two positions at Slab A (center and 15 cm away), and three specimens aged in lab air [21]. Solid/ Dashed lines: 2nd order polynomial trend fits for Steel / Concrete average. Triangle: h-axis intercepts; Steel: 0.56 mm; Concrete: 0.57 mm.

Figure 7 – Potential profiles obtained in reinforced concrete slabs illustrating overall trends and variation between replicate slabs A and B.

Figure 8 – Correlation between potentials measured with the SCE (always on a pre-wetted concrete surface) and the KP on the concrete surface in the dry and wet conditions, illustrating overall trends and variation between replicate slabs A and B.

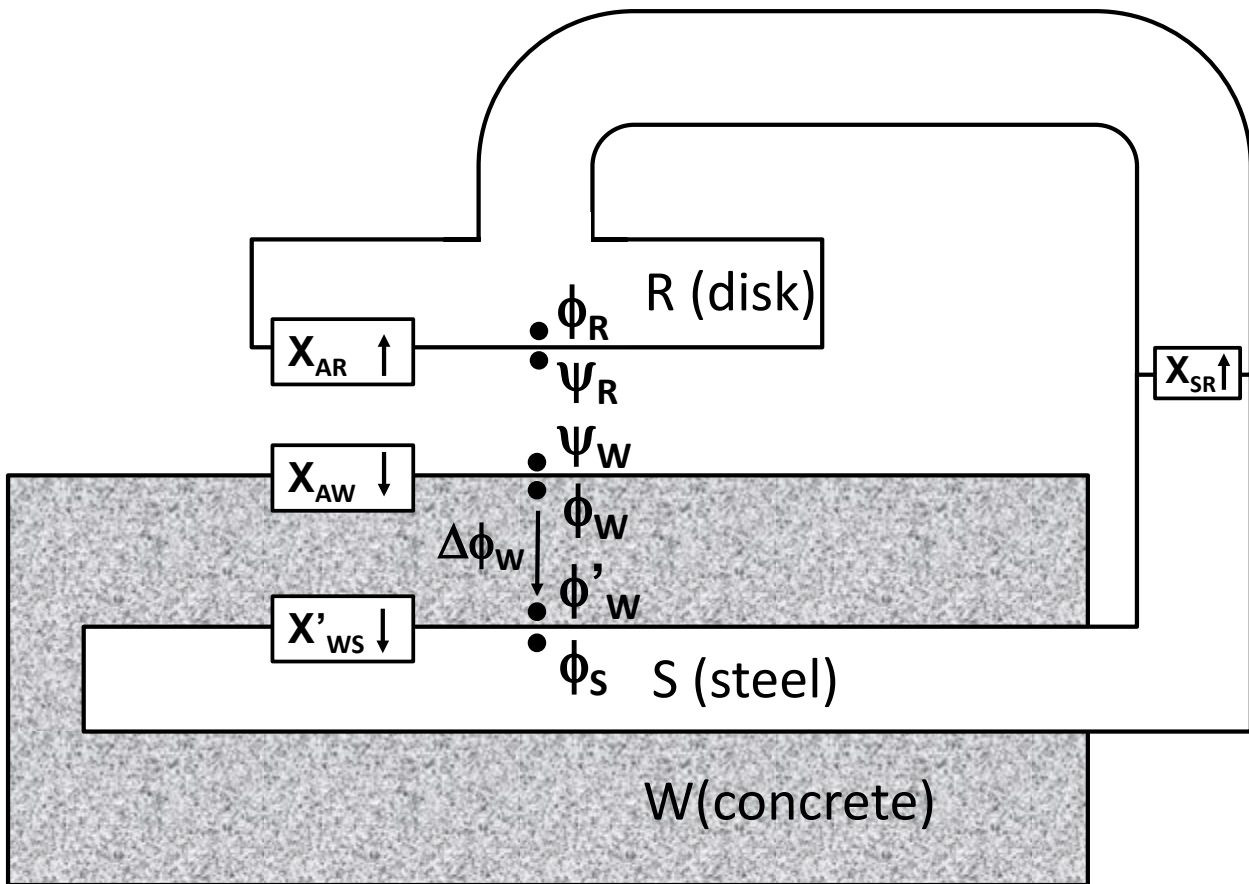


Figure 1 – Schematic representation of potentials and interfacial potential differences in a KP arrangement for steel in concrete.

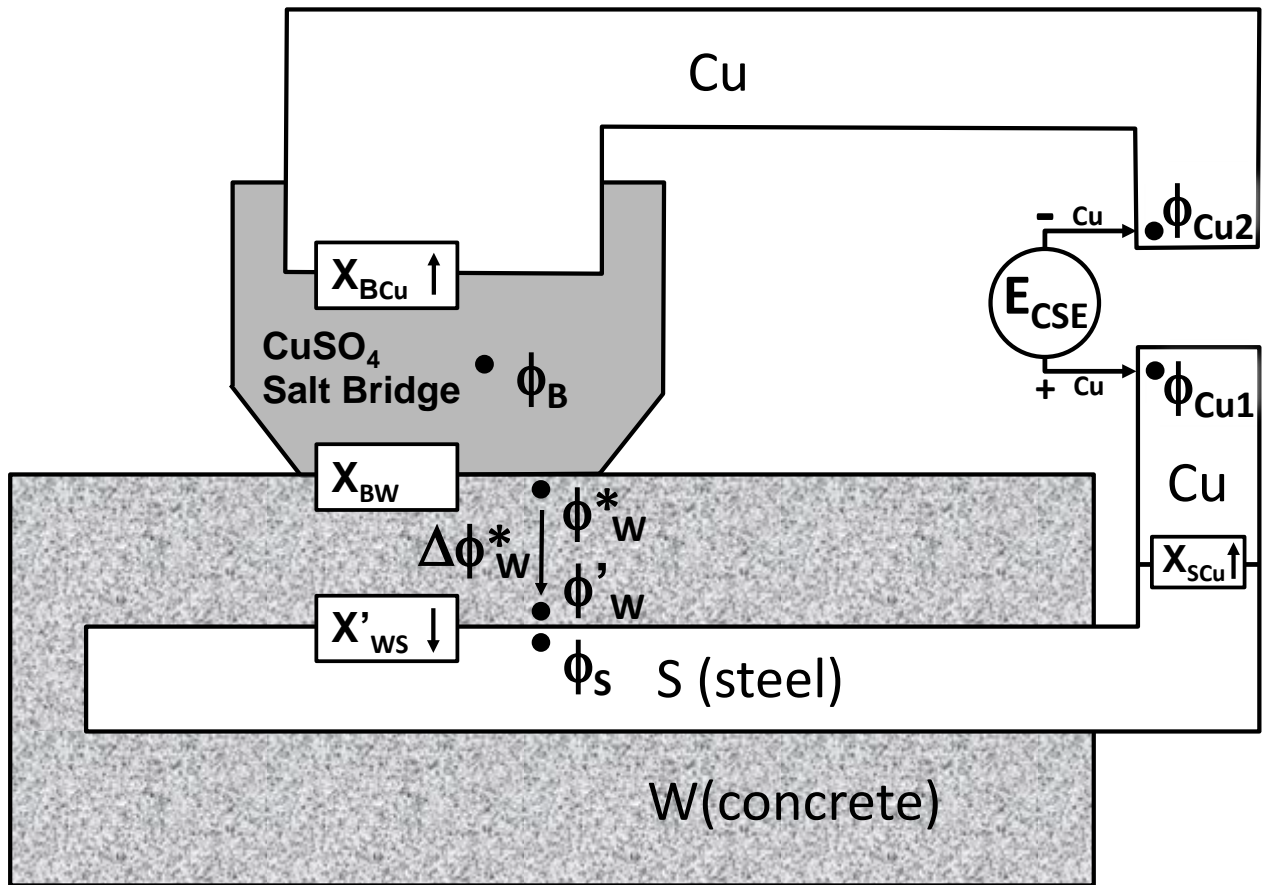


Figure 2 – Schematic representation of potentials and interfacial potential differences in a conventional reference electrode arrangement for steel in concrete, illustrated for the CSE.

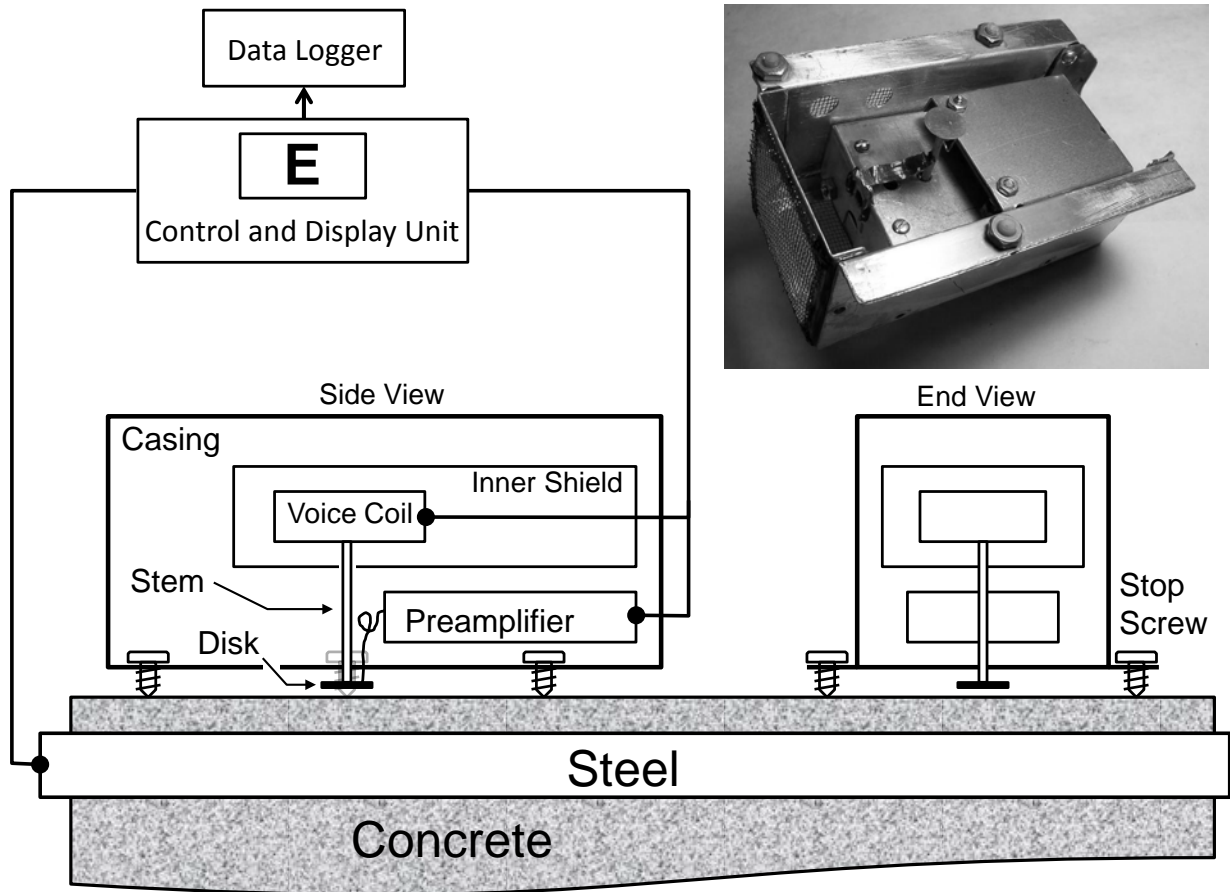


Figure 3 – Schematic and photograph of Kelvin Probe (KP) implementation.

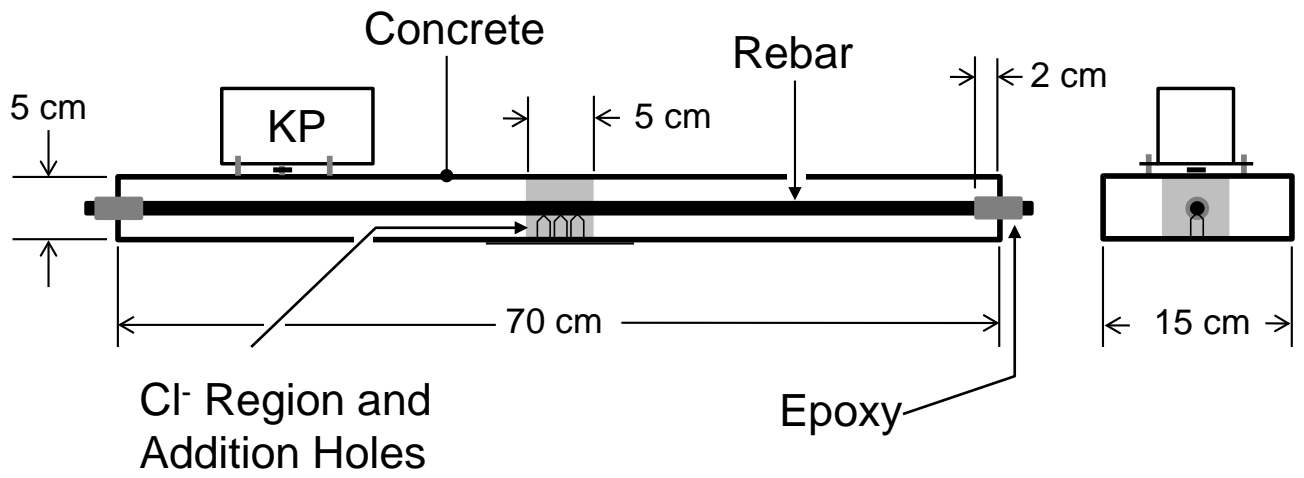


Figure 4 – Reinforced concrete test specimen configuration and example of KP probe placement.

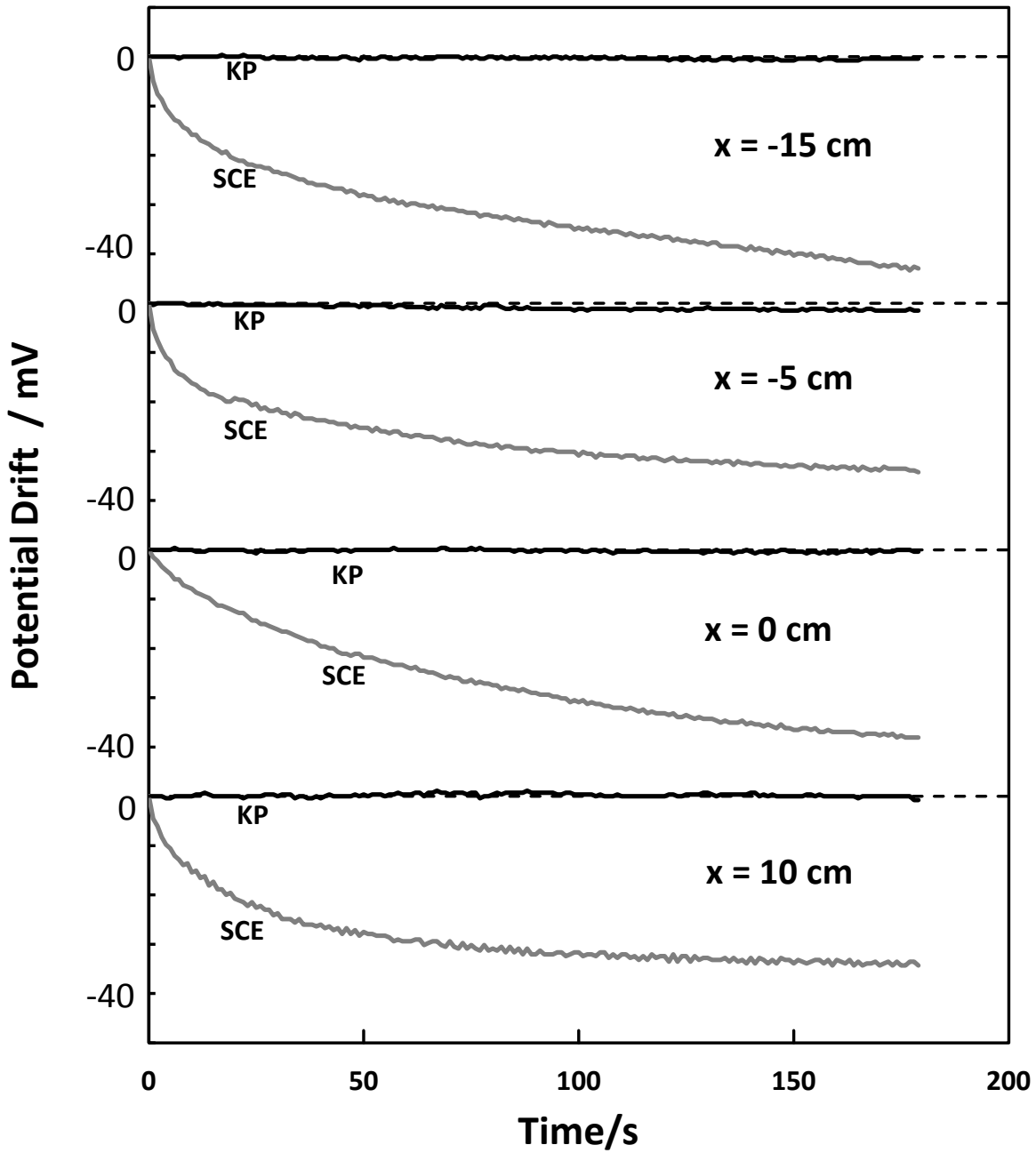


Figure 5 – Stability of Measured Potential for KP and SCE, shown as drift from value measured 1 second after probe placement on dry concrete. Results shown as stacked graphs for four positions indicated by distance from center of Slab A.

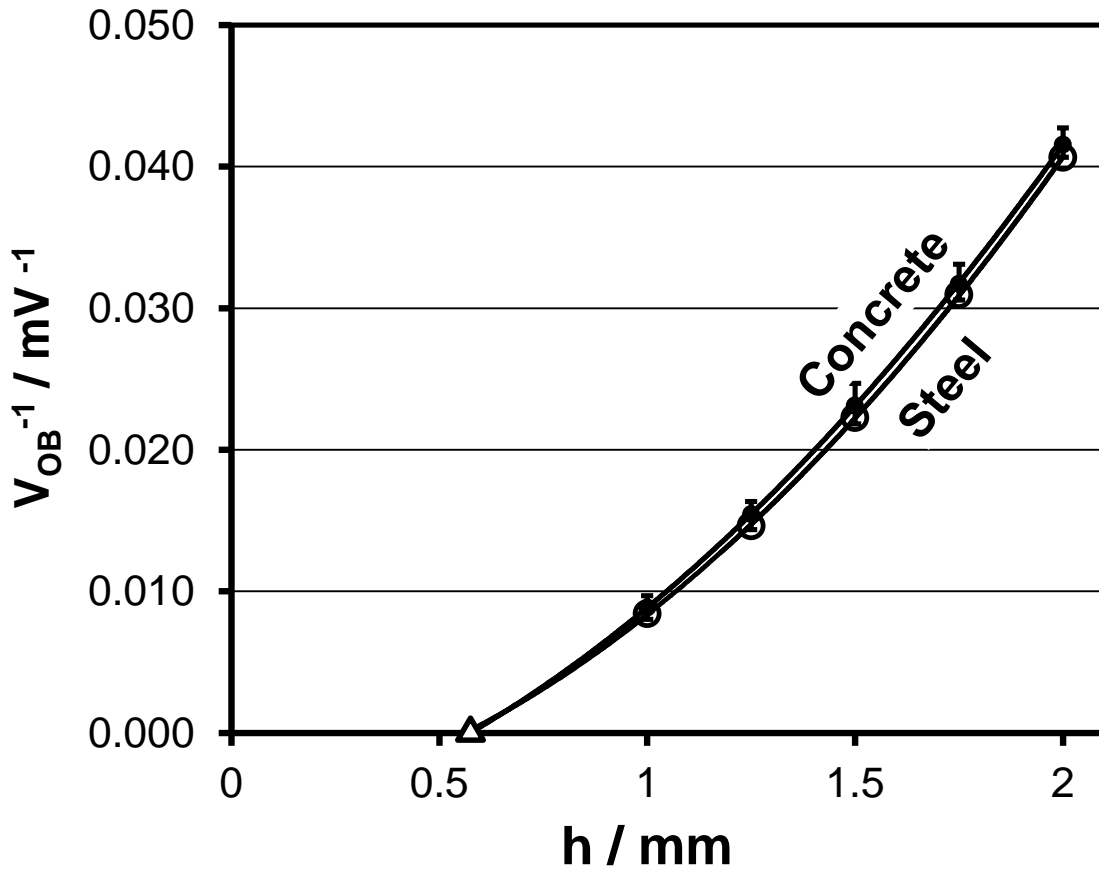


Figure 6 – Determination of effective working surface position. Circles: Flat-machined steel surface. Range bands: Two positions at Slab A (center and 15 cm away), and three specimens aged in lab air [21]. Solid/ Dashed lines: 2nd order polynomial trend fits for Steel / Concrete average. Triangle: h-axis intercepts; Steel: 0.56 mm; Concrete: 0.57 mm.

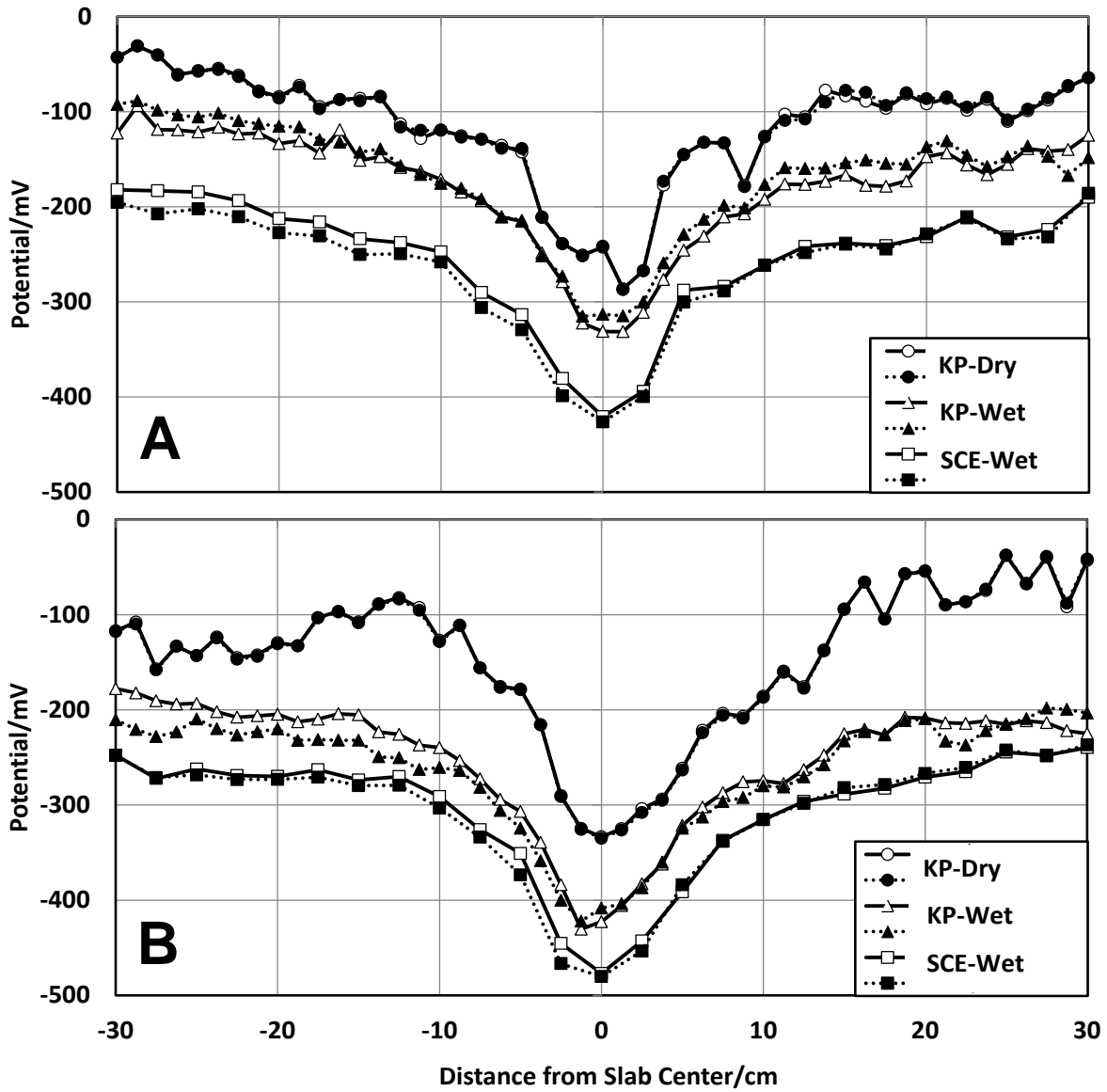


Figure 7 – Potential profiles obtained in reinforced concrete slabs illustrating overall trends and variation between replicate slabs A and B.

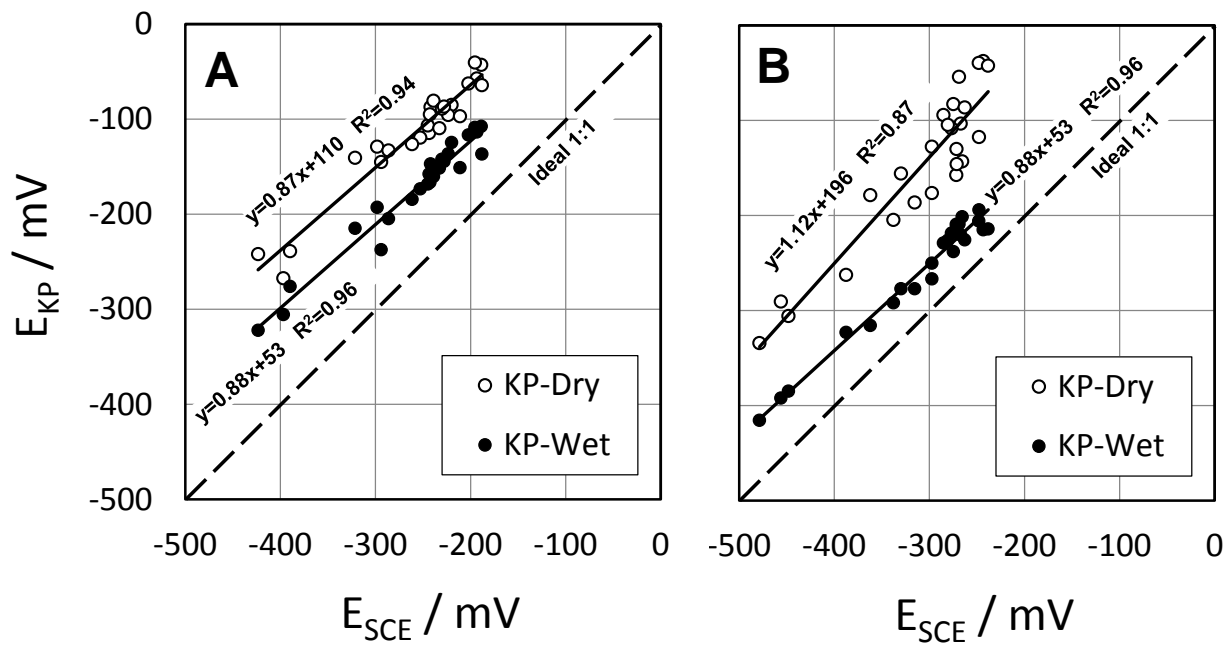


Figure 8 – Correlation between potentials measured with the SCE (always on a pre-wetted concrete surface) and the KP on the concrete surface in the dry and wet conditions, illustrating overall trends and variation between replicate slabs A and B.